INFORMATICA, 2011, Vol. 22, No. 3, 435–445

Ring Line Mapping and Rotation Inertial for Fingerprint Identification

Ching-Liang SU

Department of Industrial Engineering and Technology Management, Da Yeh University
168 University Road, Dacun, Chang-Hua 51505, Taiwan
e-mail: cls2@mail.dyu.edu.tw

Received: March 2009; accepted: October 2010

Abstract. This study uses the r-theta transformation technique to map a fingerprint image to the straight-line signals. Subsequently, the "vector magnitude invariant transform" technique is applied to them to generate an invariant magnitude for person identification. This technique can solve the image rotation problem. Various vertical magnitude strips are generated to deal with the image-shifting problem. The algorithm developed in this study can precisely classify the fingerprint images.

Keywords: ring line mapping, rotation invariant, and fingerprint identification.

1. Introduction

In the past thirty years, researchers have devoted much attention to the identification of fingerprints. The techniques used have included directional histogram equalization (Bouchaffra and Amira, 2008), binary image stream angle (Cappelli *et al.*, 2007; Lee and Choi, 2007; Nandakumar *et al.*, 2007; Bartkutė-Norkūnienė, 2009; Ross *et al.*, 2007), principal component analysis (Dagher and Nachar, 2006; Zuo and David Zhang, 2006), bright indicator (Fernandez and Fierrez, 2007), sine component mapping (Lipeika, 2010), the IFFT filter, minutia location shape matching (Galy *et al.*, 2007; Jea and Govindaraju, 2005), fine binary (Ji and Yi, 2007), orientation estimation (Jiang, 2005), the Gabor filter (Fernandez and Fierrez, 2007; Lee and Choi, 2007), feature learning (Bastys *et al.*, 2010; Tan *et al.*, 2005), wavelet transform, phase correlation (Ito *et al.*, 2005), singular point detection (Bartkutė-Norkūnienė, 2009; Jea and Govindaraju, 2005), wavelet, FFT, log polar transform, quad tree (Krašnjak and Krivec, 2005), directional detection (Fernandez and Fierrez, 2007; Park and Park, 2005), sub band decomposition, dilate enhancement, feature extraction, ridge tracing, and linear discriminate analysis (Zuo and David Zhang, 2006).

In the aforementioned research, the researchers used a very complicated mathematical mode, e.g., image phase, to solve the image rotation problem. The wavelet transform does not work well for filtering the noises plaguing a fingerprint image. The popular techniques to recognize fingerprint images were image subtraction, wherein there are two images:

one was called the "sample image" and another, "unknown image", by the subtraction of the former to the latter to recognize different fingerprints.

For comparison between the method proposed in this study and other image rotation approach, to the minutia image, for dealing with the image-shifting problem, the other method needs to locate the bifurcation point(s) of minutia image; next, the algorithm can use it as the centroid by which to extract the fingerprint image; subsequently, image rotation and comparison can be conducted to identify different images. However, in some minutia image there is no bifurcation point and/or they are very obscure, to which one cannot precisely locate them. Furthermore, the bifurcation point might locate near the end of the image frame, to which only small region of the fingerprint image can be extracted; thereby, resulting in poor comparison result. Moreover, fingerprint image might rotate to other directions with sub-pixel, greater than 15 degree, or more severe rotations. To this, sub-pixel level comparisons are required to obtain the correct comparison result; subsequently, huge amount of computation time are needed to complete the job. In addition, various number of the bifurcation points might be presented in one image, to which a image might posses its unique database to record the bifurcation sub-patterns; furthermore, one-to-many comparison technique is required to obtain the correct comparison result. To this, the system is more complicated.

The method proposed in the study can accomplish the aforementioned approach in a more efficient way. First it locates the centroid of the image; then, it performs the circle signal extraction technique which extracting the fingerprint signals and it can extract a greater region than the aforementioned method; next, it performs the rotation invariant transform which can deal with the sub-pixel and/or more than 15 degree or severe rotation problem and it only requires one computation time which is a time saving technique. For managing the image-shifting problem, the neighboring 8 pixels of the centroid are selected to run the aforementioned procedure by the try-and-error approach. To this, it is a fix-point model which can be easier to be implemented comparing to the aforementioned method.

In the present study, the image-scaling problem is ignored, i.e., the "sample image" and "unknown image" possess the same image size; however, for the image comparison the following two problem must be solved: (1) image shifting, and (2) rotation problems. Solving these two problems by the brutal method is a NP-Hard problem. In this study, the image used is a 128 by 128 image. Since two fingerprints need to be compared to find the differences, they need to be aligned to the same position. Suppose a sample image is located in the center of a 128 by 128 image and its orientation is in a straight position. For comparison, a unknown image needs to be shifted and rotated to the center and straight position. For accurate comparison, during the fine-tuning steps, the unknown image must be shifted up or down or rotated counter- or clock-wise to match the sample image. This approach is a time consuming process and the correct result might not be obtained.

In this study, the centroid of the image was located manually, by which one cannot exactly find the precise location of the centroid of the fingerprint image. After the image shifting, this study suppose the centroid of the unknown image is located in one of the following locations: $(64, 64)$, $(63, 63)$, $(63, 65)$, $(65, 65)$, $(65, 63)$, $(62, 64)$, $(64, 66)$, $(66, 64)$,

and $(64, 62)$. Fine-tuning is needed to shift this image to its proper position to obtain the better result. The follow steps are taken to fine-tune the position of the unknown image.

In this study, (1) the centroid of the "sample" and "unknown" images are supposed in position $(64, 64)$ and the ring to line signal-mapping technique is used to map both images. Subsequently, the "vector magnitude invariant transform" technique is used to transfer the sample and unknown images to an invariant vector magnitude; by comparing the differences of them, the algorithm can determine whether the sample and unknown images are the identical image, (2) the centroid of a "sample image" is supposed in position $(64, 64)$ and another image is located in position $(63, 63)$, $(63, 65)$, $(65, 65)$, $(65, 63)$, $(62, 64)$, $(64, 66)$, $(66, 64)$, and $(64, 62)$, respectively; the aforementioned procedure in (1) are applied again to determine whether both images are the identical image. By examining the final experimental result, it can be observed that this approach can yield good recognition rate.

Thus, the approximation method to match the centroids of the "sample" and "unknown" images can solve the image-shifting problem and the "ring-line mapping" and "vector magnitude invariant transform" techniques are used to solve the image-rotation problem.

In the previous discussion, the centroid position of a fingerprint image was found manually. In the future, other more reliable technique to detect the centroids of the fingerprint images might be developed.

The ring-line signal mapping technique is the interpolation of an image from the polar coordinate system to the x–y coordinate system. The "vector magnitude invariant transform" technique is used to transfer an image to an invariant vector magnitude, whereby to generate the signal vectors in the complex number domain.

This report consists of five sections. Section 2 shows the mechanism of the "vector magnitude invariant transform". Section 3 employees the r-theta transformation to extract the fingerprint image. Section 4 extracts the fingerprint signals by various locations and performs the signal comparison. Section 5 concludes this report.

2. Vector Magnitude Invariant Transform

In this study, signals are extracted by following a sampling circle, whereby the strengths of extracted ring signals generate emanated vectors. Next summing these vectors generates a single vector. Subsequently, the magnitude of this single vector can be determined, whereby is used to identify different persons. This ring can rotate to various orientations. However, no matter where the ring rotates, the aforementioned magnitude is unique. This indicates that although the fingerprint is rotated, after the transformation, the vector magnitude is invariant.

Figure 1 shows the ring-signals $x_0, x_1, x_2, \ldots, x_{127}$, wherein circle-centroid and signals x_0, x_1 generates an angle $\angle x_0 Centroid\, x_1$, wherein the angle is 2.81°. Similarly, signals x_1, x_2, and centroid also generate an angle $\angle x_1 Centroid\, x_2$ with angle 2.81° too, ... Similarly, every two signals and centroid generate an angle with 2.81°. Figure 2

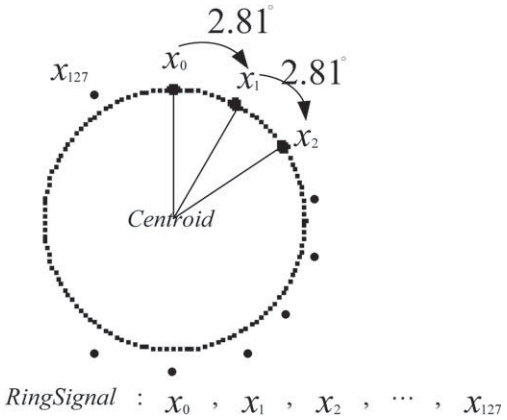

Fig. 1. Original signals.

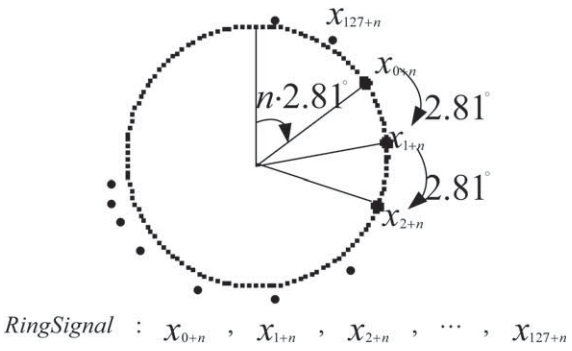

Fig. 2. Original signals rotaded $n * 2.81$ degrees clockwise.

shows the ring-signals of $x_{0+n}, x_{1+n}, x_{2+n}, \ldots, x_{127+n}$, to which every two signals and centroid also generates the angle of $2.81°$. Figures 1 and 2 present the same ring. However, the ring in Fig. 1 is rotated $n \cdot 2.81°$ clock-wisely, whereby to generate the ring of Fig. 2, wherein n is a positive integer number. Equation (1) shows the "vector magnitude invariant transform", by which to transform the signals $x_0, x_1, x_2, \ldots, x_{127}$ in Fig. 1 to vectors $f(x_0), f(x_1), f(x_2), \ldots, f(x_{127})$. Furthermore, the terms of the follows are generated: $F(u_0), F(u_1), F(u_2), \ldots F(u_{127})$. In (1) and (2), the parameter ρ is set to 2.81, since the rings in Figs. 1 and 2 contain 128 signals. The ring signals in Figs. 1 and 2 are fed to the first equation in (1) and (2) respectively, whereby $F_1(u_0)$ and $F_2(u_0)$ are generated respectively. As mentioned in the beginning of this section, the magnitudes of $F_1(u_0)$ and $F_2(u_0)$ should be equal. Therefore, $\|F_1(u_0)\|$ and $\|F_2(u_0)\|$ present the same value. Furthermore, the conclusions of follows could also be reached: $\|F_1(u_1)\| = \|F_2(u_1)\|, \ldots, \|F_1(u_{127})\| = \|F_2(u_{127})\|$. By this property, the image can be recognized, as shown in Fig. 3, whereby the orientations of them are somewhat different.

Fig. 3. Different ring signals.

$$\left.\begin{aligned}
F_1(u_0) &= f(x_0)\mathrm{e}^{-jp\cdot 0\cdot 0} + f(x_1)\mathrm{e}^{-jp\cdot 0\cdot 1} + f(x_2)\mathrm{e}^{-jp\cdot 0\cdot 2} + \cdots \\
&\quad + f(x_{127})\mathrm{e}^{-jp\cdot 0\cdot 127}, \\
F_1(u_1) &= f(x_0)\mathrm{e}^{-jp\cdot 1\cdot 0} + f(x_1)\mathrm{e}^{-jp\cdot 1\cdot 1} + f(x_2)\mathrm{e}^{-jp\cdot 1\cdot 2} + \cdots \\
&\quad + f(x_{127})\mathrm{e}^{-jp\cdot 1\cdot 127}, \\
F_1(u_2) &= f(x_0)\mathrm{e}^{-jp\cdot 2\cdot 0} + f(x_1)\mathrm{e}^{-jp\cdot 2\cdot 1} + f(x_2)\mathrm{e}^{-jp\cdot 2\cdot 2} + \cdots \\
&\quad + f(x_{127})\mathrm{e}^{-jp\cdot 2\cdot 127}, \\
&\vdots \qquad\qquad \vdots \qquad\qquad \vdots \\
F_1(u_{127}) &= f(x_0)\mathrm{e}^{-jp\cdot 127\cdot 0} + f(x_1)\mathrm{e}^{-jp\cdot 127\cdot 1} + \cdots \\
&\quad + f(x_{127})\mathrm{e}^{-jp\cdot 127\cdot 127},
\end{aligned}\right\} \tag{1}$$

$$\left.\begin{aligned}
F_2(u_0) &= f(x_{0+n})\mathrm{e}^{-jp\cdot 0\cdot (0+n)} + f(x_{1+n})\mathrm{e}^{-jp\cdot 0\cdot (1+n)} \\
&\quad + f(x_{2+n})\mathrm{e}^{-jp\cdot 0\cdot (2+n)} + \cdots + f(x_{127+n})\mathrm{e}^{-jp\cdot 0\cdot (127+n)}, \\
F_2(u_1) &= f(x_{0+n})\mathrm{e}^{-jp\cdot 1\cdot (0+n)} + f(x_{1+n})\mathrm{e}^{-jp\cdot 1\cdot (1+n)} \\
&\quad + f(x_{2+n})\mathrm{e}^{-jp\cdot 1\cdot (2+n)} + \cdots + f(x_{127+n})\mathrm{e}^{-jp\cdot 1\cdot (127+n)}, \\
F_2(u_2) &= f(x_{0+n})\mathrm{e}^{-jp\cdot 2\cdot (0+n)} + f(x_{1+n})\mathrm{e}^{-jp\cdot 2\cdot (1+n)} \\
&\quad + f(x_{2+n})\mathrm{e}^{-jp\cdot 2\cdot (2+n)} + \cdots + f(x_{127+n})\mathrm{e}^{-jp\cdot 2\cdot (127+n)}, \\
&\vdots \qquad\qquad \vdots \qquad\qquad \vdots \\
F_2(u_{127}) &= f(x_{0+n})\mathrm{e}^{-jp\cdot 127\cdot (0+n)} + f(x_{1+n})\mathrm{e}^{-jp\cdot 127\cdot (1+n)} \\
&\quad + f(x_{2+n})\mathrm{e}^{-jp\cdot 127\cdot (2+n)} + \cdots + f(x_{127+n})\mathrm{e}^{-jp\cdot 127\cdot (127+n)}.
\end{aligned}\right\} \tag{2}$$

3. Signal Mapping and Image Shifting Problem

Figure 4 shows mapping the ring signals to straight-line signals, wherein the radius of this ring is 58. This figure shows one ring generates one straight-line signal. In this study, in order to obtain more fingerprint image, various ring with different radii are used to extract fingerprint, as $13, 16, 19, 22, \ldots, 58$. Figure 5 shows the result of multiple extracted straight-lines.

Furthermore, as examining the left-picture in Fig. 4, it can be observed that the circle-center is located in position $(64, 64)$ of a 128 by 128 image, whereby the mapping straight-line signals reside in the left area in the right picture. As aforementioned, various radii are set to extract the fingerprint, as $13, 16, 19, 22, \ldots, 58$. Subsequently, the extracted results are resided in the left area, as shown in right image of Fig. 5.

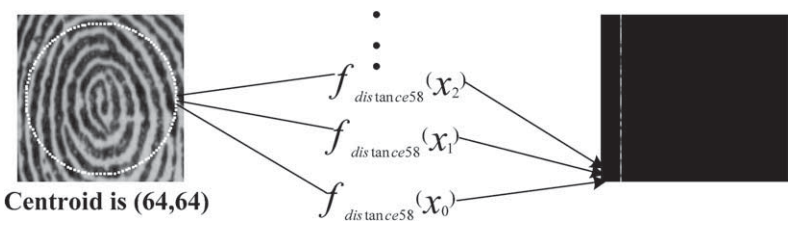

Fig. 4. Mapping ring signals to straght line signals with distance 58.

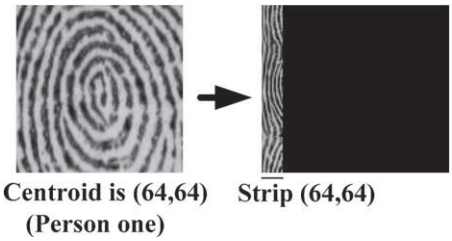

Fig. 5. Rings to lines.

It can be observed that Figs. 4 and 5 use location $(64, 64)$ as the circle-center to extract signals. For dealing with the image-shifting problem, various locations are used as the circle-centers to extract the image, as $(64, 64)$, $(63, 63)$, $(63, 65)$, $(65, 65)$, $(65, 63)$, $(62, 64)$, $(64, 66)$, $(66, 64)$, and $(64, 62)$. For each of them, the extracted signals are saved in different positions, as Figs. 6 and 7. Furthermore, for each of them, circle-radii of $13, 16, 19, 22, \ldots, 58$ are used to extract the signals. The center column pictures in Fig. 7 show the image-space is divided as the strips 0, 1, 2, . . ., and 8, wherein the aforementioned extracted strips from different circle-centers are saved. Equations (1) and (2) are applied to them to generate the results, as shown in the right column in Fig. 7.

Figure 8 shows the vertical strip comparison to identify an image. To locate the maximum matching of two images, every vertical strip in one image is compared to all of the

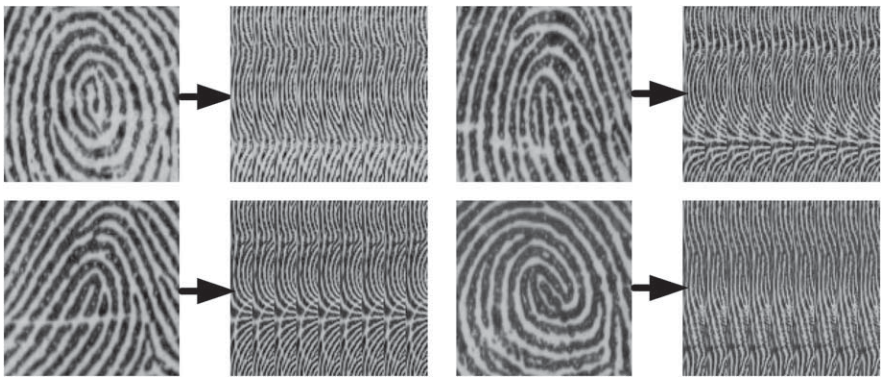

Fig. 6. Various fingerprint strips.

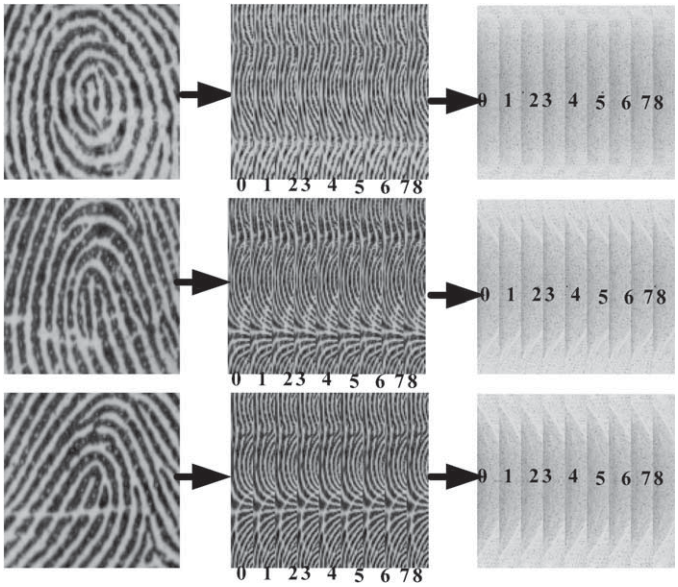

Fig. 7. Perform the vector magnitude invariant transform.

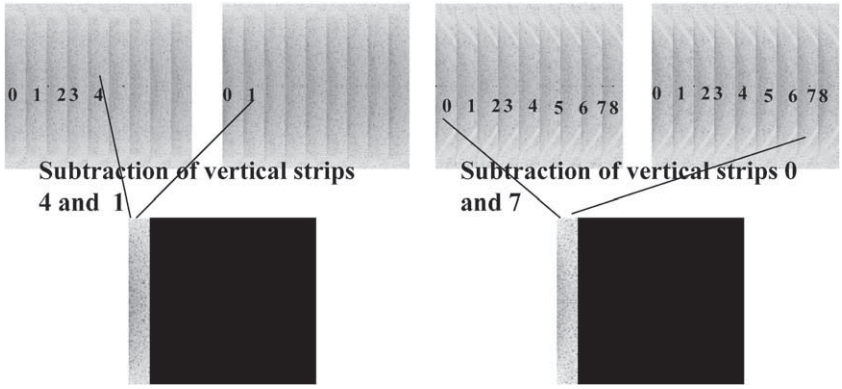

Fig. 8. Vertical strip-subtractions and results.

strips in the counter one. The left picture in Fig. 8 show the subtracted-results of strip 4 of "person one" and strip 1 of "person two"; right, strip 0, 7.

4. Results and Conclusion

In this study, three fingerprint images are taken for each person, wherein the orientations are somewhat different, and totally forty persons joining in this study for fingerprinting. The fingerprint images used in this study are 120. Considering the 120 fingerprints altogether and running them in one batch would require a very long processing time. There

is also the possibility of malfunctioning software and/or insufficient memory to accommodate the database. Therefore, the 40 participants were divided into eight groups of five persons each for testing. Since three different fingerprints were taken for each participant, 15 images were tested in each step. Thus, the system ran eight different batches.

In each group, one fingerprint was compared with the other 14 fingerprints. Altogether, 105 comparisons were conducted to test the accuracy rate. Within these comparisons, 15 were conducted for genuine comparison, since three different fingerprints were taken for each person. The other 90 comparisons were conducted to identify imposters among different fingerprints. Among the eight different test batches, there were 120 genuine tests and 720 imposter tests.

Figure 9 shows the original images. Table 1 shows partial comparison data. The data inside the rectangular boxes were the results of subtraction of two genuine fingerprints; the others, impostor. Table 2 presents the summarized results of Table 1, showing the ranges of imposter and genuine comparisons for five different persons, wherein the imposter comparison is $41\,794\,250$–$28\,431\,905$ and the correct and error ratio is $840 : 8$; for genuine, $33\,704\,838$–$11\,429\,809$, $840 : 16$.

Figure 10 shows the fine tuned binary images. As the aforementioned, Table 3 shows the partial comparison data, whereby Table 4 present the summarized results. For imposter comparisons, the range is $98\,418\,108$–$72\,385\,069$; the correct and error ratio is $840 : 8$; for genuine, $80\,497\,780$–$42\,857\,454$ $840 : 8$.

Fig. 9. Original fingerprint images.

Table 1

Comparison data

20734491	28049115	38331974	41767073	41558335	40280358	38081329	36774431	33363100	33800346	33442447	40963647	40865362	40578721
	25845059	38774807	39630665	38921547	40740182	41231314	38417736	32599301	32138165	31396717	38886745	38548097	37695333
		39655977	40076613	39920703	40294949	41565222	37841499	30115561	28431905	29050077	40123716	38850500	38708418
			26731533	33704838	36284743	36711790	36114817	37578996	37556281	37485225	34943428	34130609	34232138
				26721200	36601808	39787750	37115770	38884754	37295950	37095065	30097930	32697130	31230164
					37462533	41794250	37913380	39197896	38174797	38107238	33716521	34560855	33783499
						30957661	22670132	38481636	36666632	37300853	35430154	35062201	34426109
							28784466	40730892	40693462	41206006	39211237	38471590	38128432
								37049814	35888502	36216241	36373358	36654531	35665795
									14768049	11429809	38805435	38934819	38083381
										14153653	35531285	38370135	35880003
											35477954	37515026	36038616
												18666669	15110732
													16281327

Comparisons of identical sources

Table 2

Experiment results for original fingerprint images

	Range of comparison-values	Error range of subtracted-values	Error (times)	Error rate
Different source comparisons	41 794 250–28 431 905	28 900 000–28 431 905	8	840 : 8
Identical source comparisons	33 704 938–11 429 809	33 704 838–28 900 000	16	840 : 16

120 different fingerprints; 840 comparisons; 28 900 000 as threshod

Fig. 10. Binary fingerprint images.

Table 3

Comparison data of binary fingerprint images

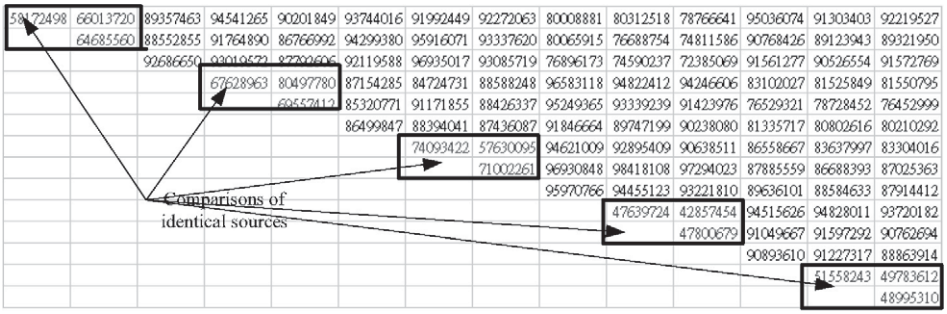

Table 4

Experiment results for binary fingerprint images

	Range of comparison-values	Error range of subtracted-values	Error (times)	Error rate
Different source comparisons	98 418 108–72 385 069	74 300 000–72 385 069	8	840 : 8
Identical source comparisons	80 497 780–42 857 454	80 497 780–74 300 000	16	840 : 8

120 different fingerprints; 840 comparisons; 74 300 000 as threshod

References

Bartkutė-Norkūnienė, V. (209). Stochastic optimization algorithms for support vector machines classification. *Informatica*, 20(2), 173–186.

Bastys, A., Kisel, A., Šalna, B. (2010). The use of group delay features of linear prediction model for speaker recognition. *Informatica*, 21(1), 1–12.

Bouchaffra, D., Amira, A. (2008). Structural hidden Markov models for biometrics: fusion of face and fingerprint. *Pattern Recognition*, 41, 852–867.

Cappelli, R., Lumini, A., Maio, D. (2007). Fingerprint image reconstruction from standard templates. *IEEE Transaction on Pattern Analysis on Machine Intelligence*, 29(9), 1489–1503.

Dagher, I., Nachar, R. (2006). Face recognition using IPCA-ICA algorithm. *IEEE Transaction on Pattern Analysis on Machine Intelligence*, 28(6), 996–1000.

Fernandez, F.A., Fierrez, J. (2007). A comparative study of fingerprint image-quality estimation methods. *IEEE Transaction on Information Forensics Security*, 2(4), 734–743.

Galy, N., Charlot, B., Courtois, B. (2007). A full fingerprint verification system for a single-line sweep sensor. *IEEE Sensors Journal*, 7(7), 1054–1065.

Ito, K., Morita, A., Aoki, T., Higuchi, T., Nakajima, H., Kobayashi, K. (2005). A fingerprint recognition algorithm using phase-based image matching for low-quality fingerprints. *IEEE Conference*.

Jea, T.-Y., Govindaraju, V. (2005). Aminutia-based partial fingerprint recognition system. *Pattern Recognition*, 38, 1672–1684.

Ji, L., Yi, Z. (2007). Binary fingerprint image thinning using template-based PCNNs. *IEEE Transaction on System, Man, and Cybernetics, Part B: Cybernetics*, 37(5), 1407–1413.

Jiang, X. (2005). On orientation and anisotropy estimation for online fingerprint authentication. *IEEE Transaction on Signal Processing*, 53(10), 4038–4049.

Krašnjak, D., Krivec, V. (2005). Fingerprint classification using a homogeneity structure of fingerprint's orientation field and neural net. In: *Proceedings of the 4th International Symposium on Image and Signal Processing and Analysis*, pp. 7–11.

Lee, C., Choi, J-Y. (2007). Alignment-free cancelable fingerprint templates based on local minutiae information. *IEEE Transaction on System, Man, and Cybernetics, Part B: Cybernetics*, 37(4), 980–992.

Lipeika, A. (2010). Optimization of formant feature based speech recognition. *Informatica*, 21(3), 361–374.

Nandakumar, K., Jain, A.K., Pankanti, S. (2007). Fingerprint-based fuzzy vault: implementation and performance. *IEEE Transaction on Information Forensics Security*, 2(4), 744–757.

Park, C.H., Park, H. (2005). Fingerprint classification using fast Fourier transform and nonlinear discriminated analysis. *Pattern Recognition*, 38, 495–503.

Ross, A., Shah, J., Jain, A.K. (2007). From template to image: reconstructing fingerprints from minutiae points. *IEEE Transaction on Pattern Analysis on Machine Intelligence*, 29(4), 544–560.

Tan, X., Bhanu, B., Lin, Y. (2005). Fingerprint classification based on learned features. *IEEE Transaction on System, Man, and Cybernetics, Part C: Applications and Reviews*, 35(3), 287–300.

Zuo, W., Zhang, D. (2006). BDPCA plus LDA: a novel fast feature extraction technique for face recognition. *IEEE Transaction on System, Man, and Cybernetics, Part B: Cybernetics*, 36(4), 946–953.

C.-L. Su in 1995 and 1993 respectively received his PhD and MS degrees in computer engineering from the University of Louisiana at Lafayette, USA. He received his MS degree in electrical computer engineering in 1989 from the University of Louisville at Kentucky, USA. In June 1982, he graduated from National Taipei University of Technology with a major in electronic engineering. From August 1995 to July 2000, he was working for the Department of Information Management, Oversea Chinese Institute of Technology, in Taiwan. From August 2000 up to now, he works in the Department of Industrial Engineering and Technology Management, Da Yeh University, in Taiwan. From April to September 2010, he visited Electrical Engineering Department, Stanford University USA, as a visiting professor. His research interest is image processing and pattern recognition.

Pirštų atspaudų identifikavimas žiedinių linijų ir rotacijos transformacija

Straipsnyje panaudota signalų r-teta transformacija modeliuojant pirštų atspaudus. Metodas gali spręsti vaizdų rotacijos problemą. Generuojami įvairūs vertikalūs rėžiai surišti su vaizdų postūmio problema. Pasiūlytas algoritmas gali tiksliai klasifikuoti pirštų atspaudų vaizdus.